GOSPODARKA SUROWCAMI MINERALNYMI – MINERAL RESOURCES MANAGEMENT

2026 Volume 42 Issue 1 Pages 141–161

DOI: 10.24425/gsm.2026.158274

CAIYUN WU[1], CHUNRONG PAN[2], KAI FENG[3], DECAN ZENG[4]

Optimized Variational Mode Decomposition combined with Wavelet Thresholding for noise reduction in magnetic induction sorting system

Introduction

China holds approximately 12% of the world's iron ore reserves (Jiang et al. 2024). In recent years, as high-grade mineral resources continue to deplete, the comprehensive utilization of low-grade minerals has become crucial for the sustainable development of the mining industry (Ponomarenko et al. 2021). Low-grade ore sorting technologies can reduce production costs for mining companies, minimize energy consumption in redundant mining

✉ Corresponding Author: Chunrong Pan; e-mail: crpan@jxust.edu.cn

[1] School of Mechanical and Electrical Engineering, Jiangxi University of Science and Technology, Ganzhou 341000, China; e-mail: CaiyunWu_study@163.com

[2] School of Mechanical and Electrical Engineering, Jiangxi University of Science and Technology, Ganzhou 341000, China; ORCID iD: 0000-0002-2239-9126; e-mail: crpan@jxust.edu.cn

[3] School of Intelligent Manufacturing and Materials Engineering, Gannan University of Science and Technology, Ganzhou 341000, China; e-mail: 7120230091@mail.jxust.edu.cn

[4] School of Mechanical and Electrical Engineering, Jiangxi University of Science and Technology, Ganzhou 341000; School of Mechanical and Electrical Engineering, Heyuan Technician Institute, China; e-mail: 7120230090@mail.jxust.edu.cn

and beneficiation processes, and effectively improve resource utilization while reducing tailings discharge (Steiner and Geissler 2018). Consequently, the development of efficient ore beneficiation technologies has become an important research direction in the field of mining engineering.

The ore beneficiation process typically consists of four sequential stages: raw ore processing, crushing, grinding, and fine separation (Yu 2004; Yang et al. 2019). To reduce energy consumption (Nedelcu and Watson 2002; Luo et al. 2022) and enhance the utilization of mineral resources, scholars have proposed various advanced mineral processing technologies. In recent years, technologies such as X-ray transmission and sensor technologies have gained popularity. Bellusci et al. used laser-induced fluorescence-based sensors combined with X-ray to perform rough sorting of Trona ore, achieving a recovery rate of 70% (Bellusci et al. 2022). Additionally, Duan et al. proposed a novel technology using microwave imaging to identify the presence of valuable minerals within ores (Duan et al. 2023). These studies provide important theoretical and technical support for the implementation of this work.

Research on magnetic sorting devices began in the mid-19th century, and with the advent of high-performance permanent magnets, these devices have evolved into permanent magnet systems (Joseph et al. 2016). Despite certain improvements in existing magnetite ore sorting devices, their levels of automation and intelligence remain suboptimal, failing to sort low-grade ores efficiently (Fariss et al. 2025). Therefore, Ren et al. developed an innovative approach that utilizes a magnetic induction sorting device for ore processing (Ren 2021). This device differs fundamentally from conventional force-field sorters by employing Hall sensors to precisely measure the magnetic field strength and determine its specific magnetic susceptibility. The magnetic induction sorting device effectively prevents the misclassification of weakly magnetic particles into tailings, thereby enhancing the efficiency of mineral resource utilization. However, sensors are susceptible to interference from external factors such as power fluctuations, electromagnetic radiation, and mechanical vibrations when collecting the magnetic induction signal, leading to random noise (Zhang et al. 2015). This noise can obscure the signals from low-grade ores and affect the accuracy of sorting. To expand the grade sorting range and improve the sorting accuracy of magnetite ore, it is necessary to select a suitable method to denoise the magnetic induction signal.

Currently, common algorithms for signal denoising include Gaussian filtering, median filtering (Zhang et al. 2016), and wavelet transform denoising methods (Zhang et al. 2022). Traditional denoising algorithms are computationally efficient; however, they exhibit limited effectiveness and adaptability when processing nonlinear and nonsmooth data. Additionally, these algorithms show poor denoising performance and may result in the loss of useful feature signals during white noise removal. To address this issue, Huang et al. introduced an adaptive signal processing method for processing nonlinear and nonsmooth signals, i.e., Empirical Mode Decomposition (EMD) (Li et al. 2025). Li et al. proposed an EMD-based multiresolution analysis method, achieving significant noise reduction in airborne LiDAR bathymetry full-waveform signals (Li et al. 2024). Xue et al. integrated ensemble empirical

mode decomposition (EEMD) and permutation entropy to objectively distinguish noise-dominated and target-dominated intrinsic mode functions in ground-penetrating radar (GPR) signals, effectively removing the noise in the GPR signal and improving the resolution of the target (Xue et al. 2019). Although these methods exhibit effective noise suppression in signal data, they are prone to modal aliasing and endpoint effects, potentially resulting in the loss of effective signals (Koppolu and Chemmangat 2023).

To address modal aliasing and effective signal loss, Dragomiretskiy and Zosso proposed the variational modal decomposition method (Dragomiretskiy and Zosso 2013). This method iteratively searches for the optimal solution of the variational model and determines the center frequency and bandwidth of each component, which is a non-recursive model. It effectively mitigates modal aliasing and endpoint effects in the EMD algorithm and demonstrates strong robustness in sampling and denoising. Geng et al. employed VMD to effectively reduce the impact of electromagnetic interference on the balance transmission module in high-speed electric multiple units (Geng et al. 2020). Gao et al. employed the SSA to optimize VMD parameters, thereby enhancing wind power prediction accuracy and reducing forecasting errors (Gao et al. 2023). Wang et al. proposed a joint denoising method based on VMD and WT, effectively addressing the noise of LiDAR echo signals and improving the inversion accuracy of LiDAR signals (Wang et al. 2022). Although VMD outperforms EMD, its denoising performance is highly influenced by the selection of algorithm parameters during signal decomposition.

In summary, to address the challenges faced by the magnetic sorting device, this study proposes a denoising framework based on SSA-VMD-WT. Specifically, SSA is employed to optimize the parameters of VMD, followed by the selection of appropriate IMFs based on sample entropy. Finally, WT is applied to perform localized and flexible denoising. The proposed method effectively suppresses signal noise and provides a robust approach for improving signal quality and separation performance in the magnetic induction sorting system.

1. Magnetic induction sorting system

1.1. The principle of signal detection

The magnetic induction sorting system employs a high-sensitivity Hall sensor to measure the magnetic field strength of magnetite ore. The operating principle of Hall sensors relies on the Hall effect (Wang et al. 2018). When a current flows through a conductor perpendicular to an external magnetic field, a potential difference known as the Hall voltage is generated across the conductor.

Based on this principle, when magnetite ore passes through the Hall sensor, the sensor converts the ore's magnetic field strength into a voltage signal, which exhibits

a linear relationship with the magnetic field intensity − a higher voltage indicates stronger magnetization. This relationship allows for the determination of the specific magnetic susceptibility of magnetite, which is essential for ore separation.

1.2. Working principle of sorting system

The modified magnetic induction sorting system is shown in Figure 1.

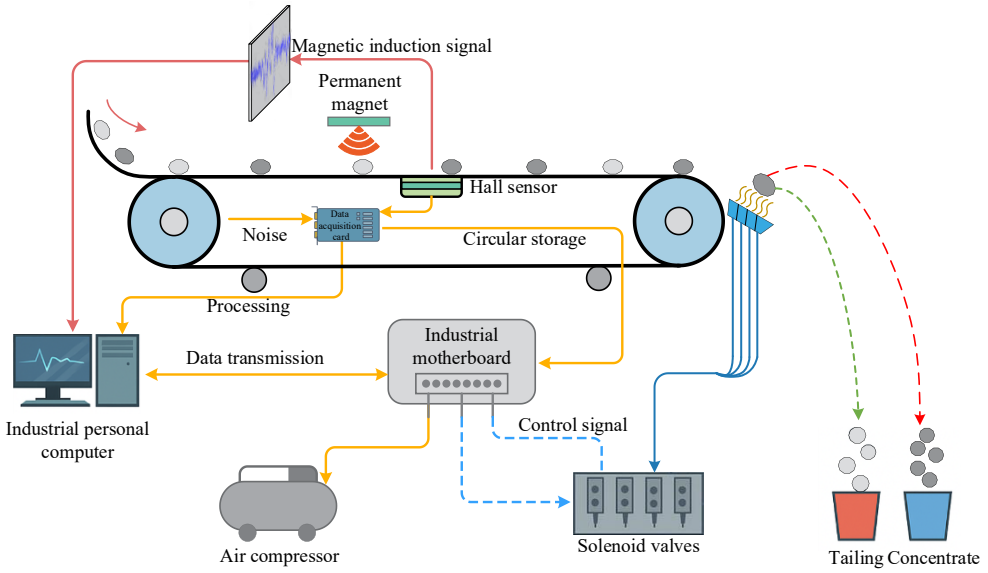

Fig. 1. Magnetic induction sorting system

Rys. 1. System sortowania indukcyjnego magnetycznego

The proposed sorting system consists of customized Hall sensors, a data acquisition card, a vibrating feeder, industrial control motherboards, a conveyor belt, solenoid valves, and NdFeB permanent magnets. The system architecture is divided into five functional modules. Specifically, the Magnetization Module uses NdFeB permanent magnets to magnetize ores, thereby enhancing their magnetic field strength and amplifying the signal peak; The Signal Detection and Acquisition Module uses Hall sensors to collect the magnetic induction signals of magnetite ores and convert them into voltage signals; The Signal Processing and Recognition Module consists of a personal computer and industrial motherboards, which perform noise reduction, analysis, and recognition of the collected signals; The Execution Module controls the solenoid valve to perform the jet action, thus separating the concentrate from the waste ore. The Remote Monitoring Module monitors the magnetic induction signals collected by the sensors on the personal computer to facilitate system debugging.

Before grinding, the particle size of magnetite ore typically ranges from 10 to 30 mm. To prevent ore losses in the separation process, each Hall sensor array comprises 24 probes with a center-to-center spacing of 10 mm. In this study, the Hall sensors with a sensitivity of 50 mV/GS are employed to ensure effective detection of the magnetic induction signals of the magnetite ore. Moreover, the conveyor belt is set to a length of 4 m to ensure that the ore remains stable when passing through the sensor and to improve the accuracy of data collection. Additionally, a circular buffer algorithm is implemented within the industrial control motherboard to ensure the continuous delivery of trigger signals, thus enabling uninterrupted ore sorting. The magnetic sorting device is shown in Figure 2.

Fig. 2. Magnetic induction signal detection platform
(a) experimental platform, (b) industrial control motherboard, (c) Hall sensor

Rys. 2. Platforma wykrywania sygnałów indukcji magnetycznej
(a) platforma eksperymentalna, (b) płyta główna sterowania przemysłowego, (c) czujnik Halla

The permanent magnet is installed above the conveyor belt, and the sensor is positioned below the conveyor belt, close to the pneumatic nozzle. Since the magnetic field intensity generated by the magnetite decreases with increasing distance, the sensor should be positioned as close as possible to the ore to ensure optimal detection performance. Additionally, to prevent friction between the sensor and the conveyor belt from affecting data accuracy, the sensor is installed 8 mm below the belt, with permanent magnets placed 30 mm above.

The system workflow is as follows: First, when the magnetite ore passes above the Hall sensor, the magnetization module magnetizes the ore, aligning the magnetic moments internally. Subsequently, the Hall sensor collects the magnetic induction signals and transmits the analog signals to the data acquisition card, where they are converted into digital signals and sent to the industrial computer for data normalization and signal denoising. Finally, the industrial motherboard uses thresholding methods to identify qualified ores and releases a trigger signal via a circular memory buffer.

2. Theory of algorithms

2.1. VMD algorithm

In the process of magnetite ore detection using Hall sensors, the acquired signals typically exhibit non-stationary and nonlinear characteristics due to the heterogeneous distribution of magnetic minerals and dynamic measurement conditions. These magnetic signals contain rich low-frequency components reflecting ore magnetization properties, superimposed with high-frequency anomalies induced by localized ferromagnetic concentrations. However, the raw measurements are inevitably corrupted by complex noise interference: Low-frequency vibrations come from the mechanical oscillations of the sensor platform, such as the device frame and conveyor belts. Meanwhile, high-frequency electromagnetic interference from industrial environments causes stochastic perturbations, such as power converters and heavy machinery. In this study, VMD is employed for preliminary signal denoising.

VMD is a signal decomposition method based on the variational principle and time-frequency analysis (Wei et al. 2022; Zhao et al. 2022). It decomposes complex, nonsmooth signals into multiple IMFs, which can be treated as independent signal components corresponding to different frequencies with limited bandwidth. The VMD decomposition process is a solution to a variational problem (Wang et al. 2020), i.e.,

$$\min_{\{u_k\},\{w_k\}} \left\{ \begin{array}{c} \sum_{k=1}^{K} \left\| \partial_t \left[\left(\delta(t) + \frac{j}{\pi t} \right) \cdot u_k(t) \right] e^{-jw_k t} \right\|_2^2 \\ s.t \quad \sum_k u_k(t) = f(t) \end{array} \right\} \tag{1}$$

- $u_k(t)$ – modal function obtained through decomposition,
- w_k – corresponding center frequency,
- $\sigma(t)$ – the gradient operator,
- k – number of modal components.

A quadratic penalty term α and a generalized Lagrangian multiplier λ are introduced to convert the constrained variational problem into an unconstrained one (Eequation 2), which is solved iteratively using the alternating direction multiplier method. The specific flow of VMD is shown in Figure 3.

$$\begin{aligned} L\left(\{u_k\},\{w_k\},\lambda\right) = \alpha \sum_{k=1}^{K} \left\| \partial_t \left[\left(\delta(t) + \frac{j}{\pi t} \right) \cdot u_k(t) \right] \mathrm{e}^{-\mathrm{j}w_k t} \right\|_2^2 \\ + \left\| f(t) - \sum_{k=1}^{K} u_k(t) \right\|_2^2 + \left\langle \lambda(t), f(t) - \sum_{k=1}^{K} u_k(t) \right\rangle \end{aligned} \tag{2}$$

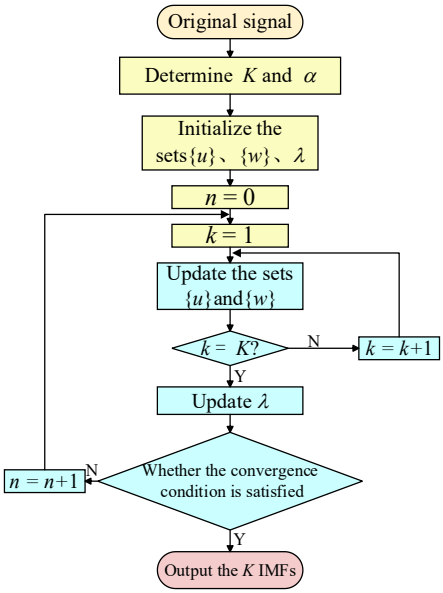

Fig. 3. VMD decomposition process

Rys. 3. Proces dekompozycji VMD

2.2. SSA and sample entropy analysis

From Eequation 2, the performance of VMD decomposition is primarily governed by the parameters K and α. An excessively large K may result in signal over-decomposition and increased computational complexity, whereas an insufficiently small K may lead to inadequate denoising. Additionally, the penalty factor α influences the bandwidth of the decomposed modes and impacts the accuracy of signal reconstruction. In practical applications, the performance of VMD decomposition may be suboptimal due to the empirical selection of K and α. Consequently, identifying the optimal combination of K and α is critical for effective VMD decomposition. This study proposes using the SSA to optimize VMD parameters, eliminating the impact of human subjectivity and enabling efficient identification of optimal parameter combinations.

The SSA is a nature-inspired stochastic optimization algorithm known for its strong global optimization capability, rapid convergence rate, and stability. It is inspired by the social behaviors of sparrows during foraging and anti-predator activities. The algorithm simulates a sparrow population divided into three distinct roles: discoverers, joiners, and warners. These roles iteratively update their positions to locate the individual with the best fitness value, which corresponds to the optimal solution (Tao et al. 2020; Zhang et al. 2024). In this study, envelope entropy is employed as the fitness function for the SSA to evaluate the

effectiveness of VMD decomposition. Envelope entropy quantifies signal complexity and uncertainty, which is particularly useful for analyzing the amplitude envelope of a signal (Yang et al. 2023). It is defined as follows:

$$p_i(t) = \frac{b_i(t)}{\sum_{t=1}^{N} b_i(t)} \tag{3}$$

$$E_i = -\sum_{t=1}^{N} p_i(t) lg\left(p_i(t)\right) \tag{4}$$

- $b_i(t)$ – envelope signal derived through the Hilbert transform of the modal component signals,
- $p_i(t)$ – probability distribution function derived by normalizing the envelope signal,
- N – temporal length of the signal series,
- E_i – computed envelope entropy for each component.

When the IMFs contain fewer noise components, their characteristic information related to the original signal becomes more distinct, and the envelope entropy decreases accordingly. In this study, the values of K and α that yield the lowest envelope entropy are obtained through iterative optimization, ensuring that the resulting IMFs retain the maximum characteristics of the ore's magnetic signal. The optimization process is illustrated in Figure 4.

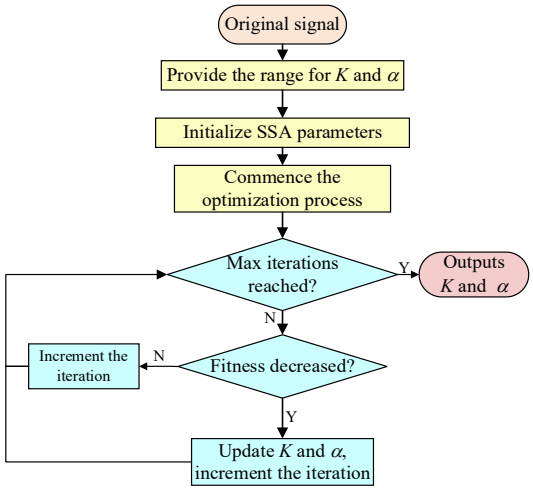

Fig. 4. Flow of SSA parameter optimization

Rys. 4. Przebieg optymalizacji parametrów SSA

After VMD decomposition with the optimal parameters, the sample entropy of each IMF is calculated. Sample entropy serves as a nonlinear indicator for quantifying time series complexity. It reveals irregularities and disorder in a time series by comparing the similarity of patterns across different embedding dimensions (Noman et al. 2022; Udhayakumar et al. 2018). The core formulation of the algorithm is as follows:

$$SampEn(m,r) = -\ln\left[\frac{B^{m+1}(r)}{B^{m}(r)}\right] \tag{5}$$

- $B^m(r)$ – similarity match of a subsequence of length m.

Typically, a higher sample entropy value means that the modal component is disordered noise, leading to the removal of modal components with larger sample entropy values. The retained IMFs represent the dominant signal components with minimal information loss. Subsequently, wavelet thresholding is employed to denoise the retained IMFs.

2.3. WT algorithm

The WT denoising method is a signal denoising method based on the wavelet transform (He and Tan 2018). The method initially selects an appropriate wavelet basis and decomposition level to perform wavelet decomposition on the noisy signal. A threshold function is then applied to quantize the wavelet coefficients, followed by an inverse wavelet transform to reconstruct the denoised signal. There are two classical thresholding functions:

Definition of the hard threshold function:

$$\tilde{d}_{j,k} = \begin{cases} d_{j,k} & \left(\left|d_{j,k}\right| \geq T\right) \\ 0 & \left(\left|d_{j,k}\right| < T\right) \end{cases} \tag{6}$$

Definition of the soft threshold function:

$$\tilde{d}_{j,k} = \begin{cases} sign(d_{j,k})\left(\left|d_{j,k}\right| - T\right) & \left(\left|d_{j,k}\right| \geq T\right) \\ 0 & \left(\left|d_{j,k}\right| < T\right) \end{cases} \tag{7}$$

- $d_{j,k}$ – original wavelet coefficients of the signal,
- $\tilde{d}_{j,k}$ – denoised wavelet coefficients,
- $sign(d_{j,k})$ – sign function,
- T – threshold.

The hard thresholding function is discontinuous at the threshold point, which may cause oscillations in the reconstructed signal. In contrast, although the soft thresholding function is continuous, it introduces a constant deviation between the original and denoised coefficients. Therefore, an improved thresholding function is used to address the limitations associated with both soft and hard thresholding methods (Li et al. 2024):

$$\tilde{d}_{j,k} = \begin{cases} sign\left(d_{j,k}\right)\cdot\left[\left|d_{j,k}\right| - \sin\left(\frac{\pi}{2}\left|\frac{T-\alpha}{d_{j,k}}\right|^{\beta}\right)T\right], & \left(\left|d_{j,k}\right| \geq T\right) \\ sign\left(d_{j,k}\right)\cdot\left[\left|\frac{d_{j,k}^{\beta+1}}{T^{\beta}}\right|\cdot\left(1-\sin\left(\left|1-\frac{\alpha}{T}\right|^{\beta}\cdot\frac{\pi}{2}\right)\right)\right], & \left(\left|d_{j,k}\right| < T\right) \end{cases} \tag{8}$$

The improved function guarantees asymptotic and continuity at the threshold T, without directly forcing coefficients below T to zero. In addition, given the nonlinear and non-smooth characteristics of the magnetic induction signal acquired by Hall sensors, the heuristic threshold criterion is selected for WT denoising in this study.

3. Experiment analysis

In this study, signal analysis is conducted using MATLAB on a personal computer with eight Intel Core i5-8300H/2.30GHz/16GB/DDR4 RAM to verify the performance and feasibility of the proposed signal denoising method.

3.1. Data acquisition and analysis

In this experiment, magnetite is sourced from a mine in Liaoning Province, China. The selected particle size range (10–30 mm) represents the typical particle size distribution encountered in the magnetite sorting process. Additionally, the conveyor belt speed is set to 0.78 m/s to ensure the stable passage of ores above the sensor. Practical sorting experiments are conducted under four distinct operating conditions, corresponding to ore densities of 21.78 kg/m^2, 12.5 kg/m^2, 8 kg/m^2, and 5.12 kg/m^2, respectively. These four surface densities simulate loading conditions with varying production intensities. The sampling frequency is set to 1000 Hz to ensure the acquisition of high-resolution magnetic signals, accurately capturing the transient response as the ore passes through the sensor. During each experiment, magnetic signal acquisition is initiated when the magnetite ores approach the Hall sensor and terminates once all ore particles have passed. The detected magnetic induction signals are transmitted to the data acquisition card, with representative segments

of the recorded signals selected for analysis. The magnetic induction signals corresponding to the four ore density conditions are presented in Figure 5.

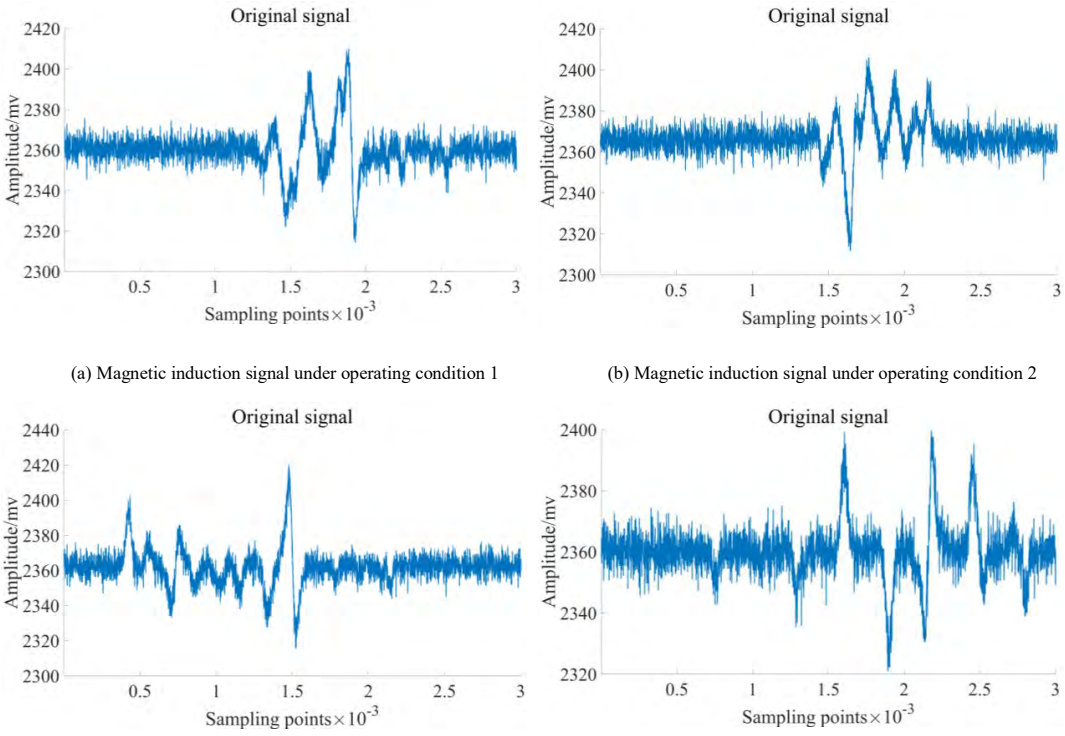

(a) Magnetic induction signal under operating condition 1

(b) Magnetic induction signal under operating condition 2

(c) Magnetic induction signal under operating condition 3

(d) Magnetic induction signal under operating condition 4

Fig. 5. The magnetic induction signals acquired under various operating conditions

Rys. 5. Sygnały indukcji magnetycznej uzyskane w różnych warunkach pracy

Considering that the signal characteristics of low-grade ore under operating condition 3 are more observable, it is selected for waveform analysis, as shown in Figure 6. The peaks and valleys correspond to the magnetic induction signal generated as magnetite ore passes through the Hall sensor. The differing directions of the peaks and valleys are attributed to variations in the magnetic moments inside the magnetite. Low-grade magnetite produces a weaker magnetic induction signal, while high-grade magnetite generates a stronger signal.

The upper and lower dashed lines in the figure represent the identification threshold lines, while the dashed line in the center represents the baseline. The wave peaks outside these dashed lines correspond to the qualified magnetic induction signals. Ore blowing conditions are triggered when the absolute difference between the waveform and the baseline

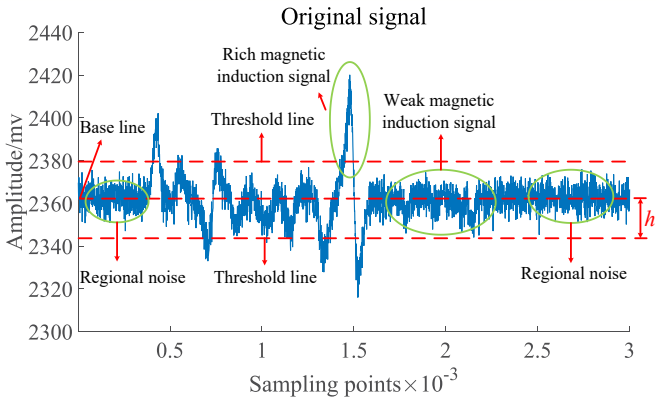

Fig. 6. Waveform analysis

Rys. 6. Analiza przebiegu falowego

surpasses the threshold interval *h*, defined as the distance between the threshold line and the baseline. If the interval of the identification threshold is too wide, the magnetic induction signal of low-grade ore may not be detected; if it is too narrow, noise may obscure the signal. Therefore, denoising is required to expand the range of recognizable ore grades.

3.2. Signal denoising process

The denoising analysis is conducted using the signal obtained under condition 3. Initially, the SSA algorithm is used to optimize the VMD parameters. In the SSA algorithm,

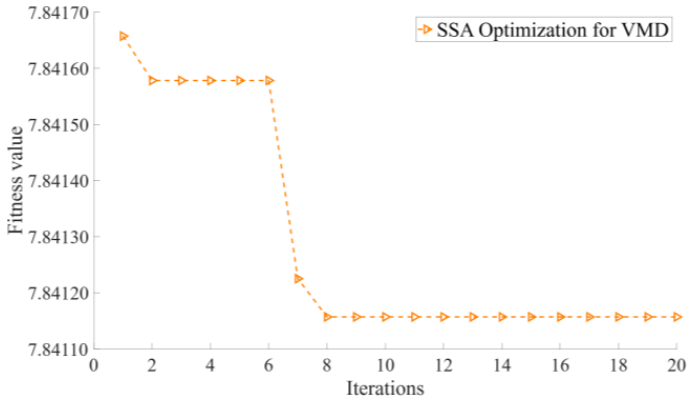

Fig. 7. SSA optimization result

Rys. 7. Wynik optymalizacji SSA

the sparrow population is set to 10, the value of k is 5–15, and the value of α is 500–3000. The fitness of the algorithm is illustrated in Figure 7. The fitness value stabilizes after the 8th iteration at 7.84115, corresponding to the optimal solution group [K, α] = [9, 2317].

VMD is performed using the optimal parameter set to obtain nine IMFs, and the frequency spectrum of the IMFs is obtained via Fast Fourier Transform (shown in Figure 8). The sample entropy value of each IMF is calculated by Eequation 5 (shown in Figure 9). If the sample entropy threshold is set too low, noise-related modal components are not removed, leading to poor initial denoising. Conversely, if the threshold is set too high,

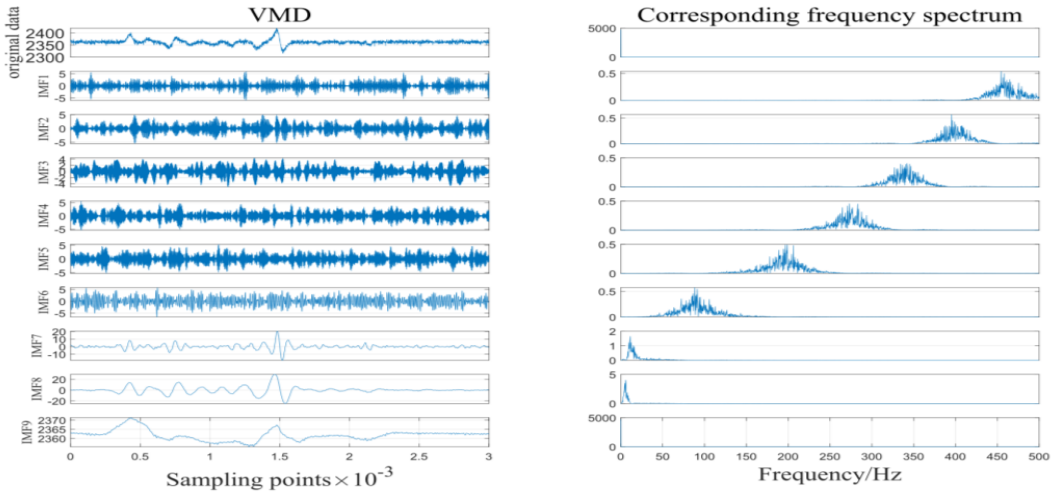

Fig. 8. VMD decomposition

Rys. 8. Dekompozycja VMD

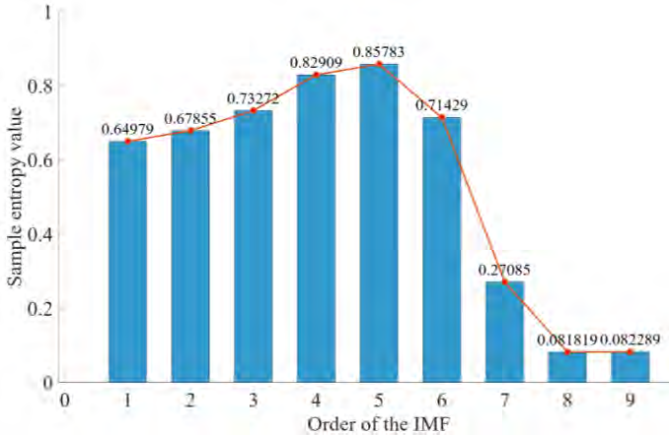

Fig. 9. Sample entropy values for each IMF

Rys. 9. Przykładowe wartości entropii dla każdego IMF

useful components of the signal may be filtered out. Based on the sample entropy values in Figure 9, IMF1-IMF6 exhibit values greater than 0.64, while IMF7-IMF9 have values below 0.28. By analyzing the sample entropy values of each IMF and the signal spectrum characteristics, it can be concluded that IMF1-IMF6 represent noisy signals, while IMF7-IMF9 represent the dominant components of the effective signal. Therefore, IMF7-IMF9 are retained for wavelet thresholding denoising, using the db5 wavelet as the basis function with a decomposition level of four (Yu et al. 2020). The denoised signal is then obtained by reconstructing the processed IMFs.

The above describes the signal denoising process, which is also applied to signals under other operating conditions. The denoised signals are shown in Figure 10.

Based on the denoising results, the proposed method effectively preserves the intrinsic characteristics of the magnetite ore waveform by suppressing noise-induced peak distortion and eliminating noise accumulation. As a result, the signal retains its essential features without observable distortion, ensuring reliable identification and classification performance, as illustrated in Figure 10.

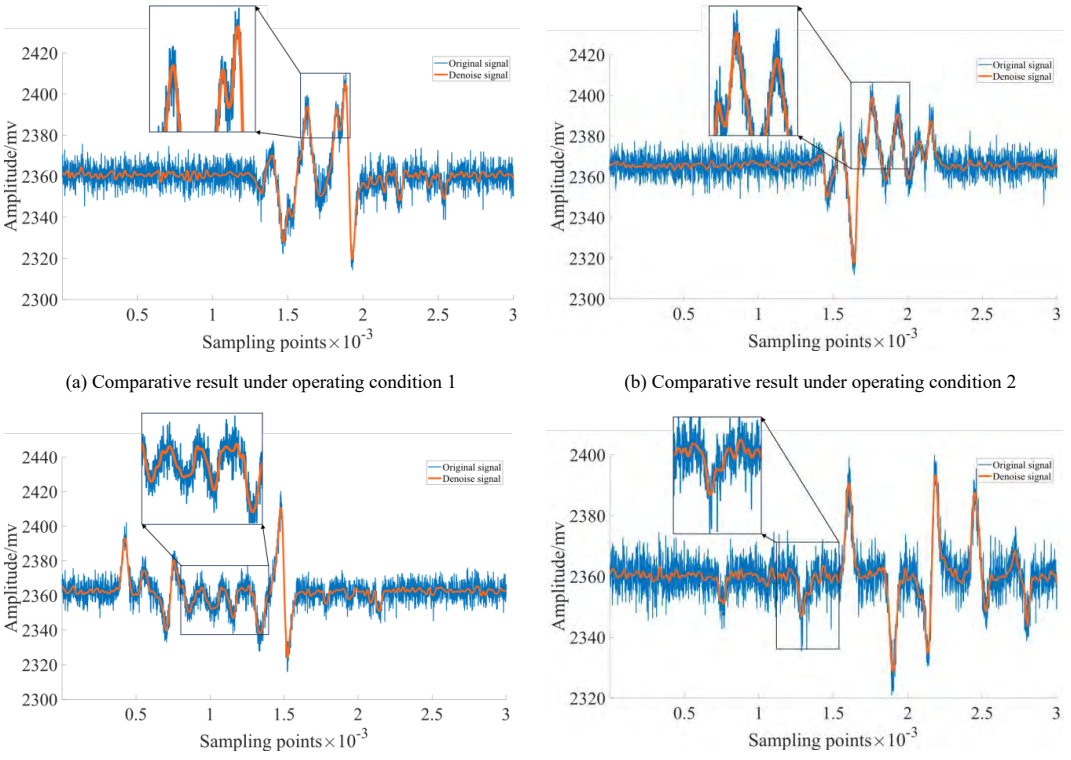

(a) Comparative result under operating condition 1

(b) Comparative result under operating condition 2

(c) Comparative result under operating condition 3

(d) Comparative result under operating condition 4

Fig. 10. Comparative analysis of the signals

Rys. 10. Analiza porównawcza sygnałów

3.3. Comparative analysis of effectiveness

The acquisition of the magnetic induction signal is influenced by environmental electromagnetic noise, vibrational noise, and other factors, making it impossible to obtain a pure signal. Therefore, to evaluate the effectiveness of signal denoising, this paper introduces two performance indicators (Ahmed et al. 2023; Yu et al. 2021) based on the characteristics of the magnetic induction signal:

Let the RVR quantify the degree of signal smoothing.

$$RVR = \sqrt{\frac{\sum_{t=1}^{n}\left(y(t+1)-y(t)\right)^2}{\sum_{t=1}^{n}\left(x(t+1)-x(t)\right)^2}} \tag{9}$$

Noise Mode (NM) quantitatively evaluates the filtering effect from an energy perspective.

$$NM = \sqrt{\sum_{t=1}^{n}\left[x(t)-y(t)\right]^2} \tag{10}$$

- $x(t)$ – original signal,
- $y(t)$ – denoised signal,
- n – number of sampling points.

This paper evaluates the denoising performance of magnetic induction signals using RVR and NM. To verify the superiority of the algorithm proposed in this study, SSA-VMD, EMD-WT, EEMD-WT, CEEMDAN-WT, and the proposed method are employed to denoise the original signals. The denoising performance of each method is presented in Table 1.

Table 1. Evaluation of denoising performance for five methods under different operating conditions

Tabela 1. Ocena skuteczności pięciu metod odszumiania w różnych warunkach pracy

Denoising methods	Condition 1		Condition 2		Condition 3		Condition 4	
	RVR	NM	RVR	NM	RVR	NM	RVR	NM
The proposed method	**0.057**	**255.163**	**0.048**	**252.782**	**0.056**	**259.152**	**0.049**	**252.246**
SSA-VMD	0.065	238.677	0.058	239.909	0.065	243.893	0.058	237.619
EMD-WT	0.071	245.675	0.062	249.275	0.062	255.305	0.065	246.255
EEMD-WT	0.068	245.789	0.056	249.258	0.063	253.811	0.057	247.372
CEEMDAN-WT	0.067	245.439	0.054	249.121	0.062	253.298	0.055	246.143

From the perspective of the signal image, the smoothness indicator quantifies the degree of signal smoothness after denoising. A lower RVR value means a smoother signal. The proposed method achieves the lowest RVR values among the five methods under different working conditions. Compared to the other four methods, it achieves RVR reductions of 14.6%, 19.2%, 13.9%, and 11.8%, respectively, with an average reduction of 14.9%. This means that the proposed method not only preserves more detailed information but also significantly enhances signal smoothness.

From the energy perspective, a larger NM means a greater amount of removed Noise. Under different working conditions, the proposed method achieves the highest NM values among the five methods. Compared to the other four methods, NM demonstrates improvements of 6.2%, 2.3%, 2.3%, and 2.5%, respectively, with an average improvement of 3.3%. This means that the proposed method achieves the best denoising performance while maximizing the retention of effective signals.

3.4. Ore sorting experiments

The experiments are conducted using 722 magnetite ore samples, with the conveyor belt speed set at 0.78 m/s. To ensure system stability, the threshold h must be set greater than the noise threshold, which is determined through statistical analysis of noise peaks observed in a large number of experimental samples. If the threshold h is set too low, random noise could be misidentified as a valid ore signal, leading to unnecessary triggering of the blowing action. Therefore, the value of h is set to match the noise threshold to minimize false triggers and effectively separate low-grade ore.

In the absence of the denoising algorithm, the noise threshold is determined through the analysis of experimental waveforms (Section 3.1), with the h set to 16 mV. Initially, magnetite ore samples that meet the blowout conditions are screened and labeled, followed by ore sorting experiments. To facilitate the collection and analysis of sorted ores, a sorting box is placed beneath the nozzle, divided into tailing and concentrate regions. After the experiment, the number of ores in the two regions is recorded separately.

After employing the denoising algorithm in the industrial control system, experiments are conducted using ore samples from the same batch, and the ore quantity and conveyor belt speed are maintained constant. Based on the analysis of experimental waveforms, the noise has been effectively suppressed, so the threshold h is set to 7 mV. Ore samples that meet the blowing conditions are screened, labeled, and then subjected to ore sorting experiments. The ore quantity in each region is recorded at the end of the experiment, with the relevant results presented in Table2.

As shown in Table 2, 134 ore pieces meet the blowing conditions in the unfiltered experiment, with an average sorting accuracy of 70.4%. After filtering, 186 ore pieces meet the blowing conditions, with an average sorting accuracy of 82.9%, representing increases of 38.8% and 12.5%, respectively. Additionally, the mis-spraying rate decreased by 10.7%.

Table 2. Ore sorting experimental results

Tabela 2. Wyniki eksperymentów dotyczących sortowania rudy

No.	Filtering employed	Minimum threshold difference	The number of ore samples meeting blowing conditions	Blown labeled ore samples	Blown unlabeled ore samples	Accuracy	False blow rate
1	No	16	134	99	13	73.9%	13.1%
2				90	15	67.2%	16.7%
3				95	11	70.1%	8.2%
4	Yes	7	186	153	3	82.2%	1.6%
5				161	4	86.6%	2.2%
6				149	4	80.1%	2.2%

Conclusion

A magnetic induction sorting system based on Hall sensors is developed to improve the detection and classification of magnetite ore. To mitigate the impact of noise interference on signal quality and sorting accuracy, a signal denoising method−SSA-VMD-WT has been proposed. Experimental results demonstrate that the proposed method significantly improves signal quality, as evidenced by notable improvements in RVR and NM metrics. Furthermore, it increases the detectable range of magnetite ore by 38.8%, increases sorting accuracy by 12.5%, and reduces the misclassification rate by 10.7%. These findings confirm that the proposed method effectively suppresses noise in the magnetic signals collected by the Hall sensor, enhancing the grade sorting range and sorting accuracy of the magnetite ore. This approach provides a reliable and effective solution for signal denoising in a magnetic induction sorting system.

This work was supported by the National Natural Science Foundation of China (NSFC) under Grant No. (72161019), Science and Technology Research Project GJJ2203618.

The Authors have no conflict of interest to declare.

REFERENCES

Ahmed et al. 2023 − Ahmed, R., Mehmood, A., Rahman, M.M.U. and Dobre, O.A. 2023. A deep learning and fast wavelet transform-based hybrid approach for denoising of PPG signals. *IEEE Sensors Letters* 7(7), pp. 1−4, https://doi.org/10.48550/arXiv.2301.06549.

Bellusci et al. 2022 − Bellusci, N., Taylor, P., Spiller, D. and Braman, V. 2022. Coarse beneficiation of trona ore by sensor-based sorting. *Mining, Metallurgy & Exploration* 39(5), pp. 2179−2185, https://doi.org/10.1007/s42461-022-00665-2.

Dragomiretskiy, K. and Zosso, D. 2013. Variational mode decomposition. *IEEE Transactions on Signal Processing* 62(3), pp. 531−544, https://doi.org/10.1109/TSP.2013.2288675.

Duan et al. 2023 − Duan, B., Bobicki, E. and Hum, S. 2023. Application of microwave imaging in sensor-based ore sorting. *Minerals Engineering* 202, https://doi.org/10.1016/j.mineng.2023.108303.

Fariss et al. 2025 − Fariss, A.H.B., Ibrahim, A.I.I., Ozdemir, A.C., Top, S., Kursunoglu, S. and Altiner, M. 2025. Beneficiation of low-grade iron ore using a Dry-Roll magnetic separator and its modeling via artificial neural network. *Journal of Sustainable Metallurgy* 11(2), pp. 1133−1149, https://doi.org/10.1007/s40831-025-01030-5.

Gao et al. 2023 − Gao, X., Guo, W., Mei, C., Sha, J., Guo, Y. and Sun, H. 2023. Short-term wind power forecasting based on SSA-VMD-LSTM. *Energy Reports* 9(10), pp. 335−344, https://doi.org/10.1016/j.egyr.2023.05.181.

Geng et al. 2020 − Geng, Q., Wen, Y., Liu, S. and Zhang, D. 2020. A VMD based improved De-noising of onboard BTM receiving signal. *Chinese Journal of Electronics* 29(1), pp. 66−72, https://doi.org/10.1049/cje.2019.10.001.

He, H. and Tan, Y. 2018. A novel adaptive wavelet thresholding with identical correlation shrinkage function for ECG noise removal. *Chinese Journal of Electronics* 27(3), pp. 507−513, https://doi.org/10.1049/cje.2018.02.006.

Jiang et al. 2024 − Jiang, H., Liu, Y., Wang, H., Li, H. and Jiang Y. 2024. An economy-wide and environmental assessment of an imported supply shortage for iron ore: The case of China. *Economic Analysis and Policy* 83, pp. 606−617, https://doi.org/10.1016/j.eap.2024.07.002.

Koppolu, P.K. and Chemmangat, K. 2023. Automatic selection of IMFs to denoise the sEMG signals using EMD. *Journal of Electromyography and Kinesiology* 73, https://doi.org/10.1016/j.jelekin.2023.102834.

Lessard et al. 2016 − Lessard, J., Sweetser, W., Bartram, K., Figueroa, J. and McHugh, L. 2016. Bridging the gap: Understanding the economic impact of ore sorting on a mineral processing circuit. *Minerals Engineering* 91, pp. 92−99.

Li et al. 2024 − Li, S., Zhu, X. and Zhou, D. 2024. Power quality disturbance signal denoising and detection based on improved DBO-VMD combined with wavelet thresholding. *Electric Power Systems Research* 238, https://doi.org/10.1016/j.epsr.2024.111193.

Li et al. 2024 − Li, W., Du, L., Meng, X., Liu, J., Li, Y. and Zhang, X. 2024. Adaptive denoising for airborne LiDAR bathymetric full waveforms using EMD-based multiresolution analysis. *IEEE Geoscience and Remote Sensing Letters* 21, pp. 1−5, https://doi.org/10.1109/LGRS.2024.3381271.

Li et al. 2025 − Li, C., Tian, S., Yang, K., Ye, P., Huang, W. and Ye, Z. 2025. FPGA-based design of multipoint parallel EMD for anomaly detection in acquisition system. *IEEE Transactions on Industrial Electronics* 99, https://doi.org/10.1109/TIE.2024.3525139.

Luo et al. 2022 − Luo, X., He, K., Zhang, Y., He, P. and Zhang, Y. 2022. A review of intelligent ore sorting technology and equipment development. *International Journal of Minerals, Metallurgy and Materials* 29(9), pp. 1647−1655, https://doi.org/10.1007/s12613-022-2477-5.

Nedelcu, S. and Watson, J.H.P. 2002. Magnetic separator with transversally magnetised disk permanent magnets. *Minerals Engineering* 15(5), https://doi.org/10.1016/S0892-6875(02)00043-2.

Noman et al. 2022 − Noman, K., Li, Y. and Wang, S. 2022. Continuous health monitoring of rolling element bearing based on nonlinear oscillatory sample entropy. *IEEE Transactions on Instrumentation and Measurement* 71, https://doi.org/10.1109/tim.2022.3191712.

Ponomarenko et al. 2021 − Ponomarenko, T., Nevskaya, M. and Jonek-Kowalska, I. 2021. Mineral resource depletion assessment: Alternatives, Problems, Results. *Sustainability* 13(2), pp. 862, https://doi.org/10.3390/su13020862.

Ren et al. 2021 − Ren, Y., Pan, C. and He, L. Research on identification method of magnetite ore based on convolutional neural network. *2021 IEEE International Conference on Networking, Sensing and Control (ICNSC)*, https://doi.org/10.1109/ICNSC52481.2021.9702170.

Steiner, G. and Geissler, B. 2018. Sustainable mineral resource management-insights into the case of phosphorus. *Sustainability* 10(8), https://doi.org/10.3390/su10082732.

Tao et al. 2020 − Tao, K., Xu, M. and Wang, Q. 2020. ASSA-VMD-SI and Frechet method of pipe vibration for noise reduction and leakage identification. *Measurement* 2242, https://doi.org/10.1016/j.measurement.2024.116277.

Udhayakumar et al. 2018 − Udhayakumar, K., Karmakar, C. and Palaniswami, M. 2018. Understanding irregularity characteristics of short-term HRV signals using sample entropy profile. *IEEE Transactions on Bio-Medical Engineering* 65(11), pp. 2569−2579, https://doi.org/10.1109/tbme.2018.2808271.

Wang et al. 2020 − Wang, D., Zhu, L., Yue, J., Lu, J., Li, D. and Li, G. 2020. Application of variational mode decomposition based on particle swarm optimization in pipeline leak detection. *Engineering Research Express* 2(4), https://doi.org/10.1088/2631-8695/abcc47.

Wang et al. 2022 − Wang, Z., Ding, H., Wang, B. and Liu, D. 2022. New denoising method for lidar signal by the WT-VMD joint algorithm. *Sensors* 22(16), pp. 5978-5978, https://doi.org/10.3390/s22165978.

Wei et al. 2022 − Wei, X., Feng, G., Qi, T., Guo, J., Li, Z., Zhao, D. and Li, Z. 2022. Reduce the noise of transient electromagnetic signal based on the method of SMA-VMD-WTD. *IEEE Sensors Journal* 22(15), pp. 14959−14969, https://doi:10.1109/JSEN.2022.3184697.

Xue et al. 2019 − Xue, W., Dai, X., Zhu, J., Luo, Y. and Yang, Y. 2019. A noise suppression method of ground penetrating radar based on EEMD and permutation entropy. *IEEE Geoscience and Remote Sensing Letters* 16(10), pp. 1625−1629, https://doi.org/10.1109/LGRS.2019.2902123.

Yang et al. 2019 − Yang, C., Ding, J., Jin, Y., Wang, C. and Chai, T. 2019. Multitasking multiobjective evolutionary operational indices optimization of beneficiation processes. *IEEE Transactions on Automation Science and Engineering* 16(3), pp. 1046−1057, https://doi.org/10.1109/tase.2018.2865593.

Yang et al. 2023 − Yang, Y., Liu, H., Han, L. and Gao, P. 2023. A feature extraction method using VMD and improved envelope spectrum entropy for rolling bearing fault diagnosis. *IEEE Sensors Journal* 23(4), pp. 3848–3858, https://doi.org/10.1109/JSEN.2022.3232707.

Yu, Y. 2004. Advance in iron ore dressing technology at home and abroad and their influence on iron-smelting. *The Chinese Journal of Nonferrous Metals* 14(1), pp. 47−51.

Yu et al. 2020 − Yu, Z., Chen, J., Zhang, B., Wang, D. and Jiang, H. 2020. Selection method of optimal wavelet basis function for aeromagnetic anomaly signal processing. *Journal of Coastal Research* 115, pp. 530−534.

Yu et al. 2021 − Yu, Z., Tang, J. Wang, Z. 2021. GCPS: A CNN performance evaluation criterion for radar signal intrapulse modulation recognition. *IEEE Communications Letters* 25(7), pp. 2290−2294, https://doi.org/10.1109/LCOMM.2021.3070151.

Zhang et al. 2015 − Zhang, D., Wang, M. and Sun, K. 2015. Low frequency noise characterization and signal-to-noise ratio optimization for silicon Hall cross sensors. *IEEE Journal of the Electron Devices Society* 3(4), pp. 365−370, https://doi.org/10.1109/JEDS.2015.2418794.

Zhang et al. 2016 − Zhang, L., Wang, Z., Shi, H., Long, Z. and Du, H. 2016. Chaos particle swarm optimization combined with circular median filtering for geophysical parameters retrieval from Windsat. *Journal of Ocean University of China* 15(4), pp. 593−605, https://doi.org/10.1007/s11802-016-2859-2.

Zhang et al. 2018 − Zhang, W., Wu, W., Chen, S., Zhang, J., Ling, X., Shu, W., Luo, H. and Wen, S. 2018. Photonic spin Hall effect on the surface of anisotropic two-dimensional atomic crystals. *Photonics Research* 6(6), pp. 511−516, https://doi.org/10.1364/PRJ.6.000511.

Zhang et al. 2022 − Zhang, X., Kuenzel, S., Colombo, N. and Watkins, C. 2022. Hybrid short-term load forecasting method based on empirical wavelet transform and bidirectional long short-term memory neural networks. *Journal of Modern Power Systems and Clean Energy* 10(5), pp. 1216−1228, https://doi.org/10.35833/MPCE.2021.000276.

Zhang et al. 2024 − Zhang, Z., Li, K., Guo, H. and Liang, X. 2024. Combined prediction model of joint opening-closing deformation of immersed tube tunnel based on SSA optimized VMD, SVR and GRU. *Ocean Engineering* 305, https://doi.org/10.1016/j.oceaneng.2024.117933.

Zhao et al. 2022 − Zhao, S., Chen, Y., Rehman, A.U., Liang, F., Wang, S. and Zhao, Y. 2022. Detection of interturn short-circuit faults in DFIGs based on external leakage flux sensing and the VMD-RCMDE analytical method. *IEEE Transactions on Instrumentation and Measurement* 71, pp. 1−12, https://doi.org/10.1109/TIM.2022.3186061.

OPTIMIZED VARIATIONAL MODE DECOMPOSITION COMBINED WITH WAVELET THRESHOLDING FOR NOISE REDUCTION IN MAGNETIC INDUCTION SORTING SYSTEM

Keywords

magnetic induction sorting system, noise interference, VMD, WT, Hall sensor

Abstract

The magnetic induction sorting system is an automated intelligent system designed specifically for magnetite ore, which can effectively separate low-grade ores. However, the magnetic induction signals detected by this system are vulnerable to noise interference, posing a significant challenge for accurate signal acquisition, thus affecting both the sorting range and accuracy. To address this issue, this study proposes a denoising method integrating the Sparrow Search Algorithm (SSA)-optimized Variational Mode Decomposition (VMD) with Wavelet Thresholding (WT). Firstly, SSA is employed to optimize the parameter configuration of VMD to achieve optimal signal decomposition. Subsequently, intrinsic mode functions (IMFs) are selectively filtered based on sample entropy analysis, and the retained IMFs undergo WT denoising. Finally, the IMFs are reconstructed to yield the denoised signal. The effectiveness of the proposed method is verified comprehensively through experiments performed with a laboratory-developed magnetic induction sorting system. Experimental results demonstrate substantial performance improvements when compared to four alternative algorithms, achieving an average improvement of 3.3% in Noise Mode (NM) and a reduction of 14.9% in Root of Variance Ratio (RVR). Moreover, the denoising algorithm led to a 38.8% increase in detectable magnetite ores and a 12.5% improvement in sorting accuracy. These results demonstrate that the proposed method effectively suppresses noise interference during the Hall sensor's collection of magnetic signals, significantly enhancing the grade sorting range and accuracy of magnetite ore.

ZOPTYMALIZOWANA DEKOMPOZYCJA MODÓW WARIACYJNYCH W POŁĄCZENIU Z PROGOWANIEM FALKOWYM W CELU REDUKCJI SZUMÓW W SYSTEMIE SORTOWANIA Z INDUKCJĄ MAGNETYCZNĄ

Słowa kluczowe

system sortowania z indukcją magnetyczną, zakłócenia szumowe, VMD, WT, czujnik Halla

Streszczenie

System sortowania z indukcją magnetyczną to zautomatyzowany, inteligentny system zaprojektowany specjalnie do analizy rud magnetytowych, umożliwiający skuteczną separację rud niskiej jakości. Sygnały indukcji magnetycznej wykrywane przez ten system są jednak podatne na zakłócenia, co stanowi poważne wyzwanie dla dokładnej akwizycji sygnału, wpływając tym samym zarówno na zakres, jak i dokładność sortowania. Aby rozwiązać ten problem, w niniejszym badaniu zaproponowano metodę odszumiania, integrującą zoptymalizowaną algorytmem wyszukiwania

Sparrow (SSA) dekompozycję modów wariacyjnych (VMD) z progowaniem falkowym (WT). Najpierw SSA jest wykorzystywany do optymalizacji konfiguracji parametrów VMD w celu uzyskania optymalnej dekompozycji sygnału. Następnie funkcje modów wewnętrznych (IMF) są selektywnie filtrowane na podstawie analizy entropii próbki, a zachowane funkcje IMF są poddawane odszumianiu metodą WT. Na koniec funkcje IMF są rekonstruowane w celu uzyskania odszumionego sygnału. Skuteczność proponowanej metody została kompleksowo zweryfikowana eksperymentami przeprowadzonymi z wykorzystaniem opracowanego w laboratorium systemu sortowania z indukcją magnetyczną. Wyniki eksperymentalne wskazują na znaczną poprawę wydajności w porównaniu z czterema alternatywnymi algorytmami, osiągając średnią poprawę o 3,3% w trybie szumu (NM) i redukcję o 14,9% współczynnika pierwiastka z wariancji (RVR). Ponadto algorytm odszumiania doprowadził do 38,8-procentowego wzrostu wykrywalności rud magnetytu i 12,5-procentowej poprawy dokładności sortowania. Wyniki te dowodzą, że proponowana metoda skutecznie tłumi zakłócenia szumowe podczas zbierania sygnałów magnetycznych przez czujnik Halla, znacząco zwiększając zakres sortowania i dokładność rudy magnetytu.